METHANE HYDRATE FORMATION AND DISSOCIATION IN A PARTIALLY SATURATED SAND — MEASUREMENTS AND OBSERVATIONS

Timothy J. Kneafsey*, Liviu Tomutsa, George J. Moridis, Yongkoo Seol, and Barry Freifeld
Lawrence Berkeley National Laboratory
Earth Sciences Division
USA

Charles E. Taylor
National Energy Technology Laboratory
Methane Hydrates Research Group
USA

Arvind Gupta
Colorado School of Mines
Center for Hydrate Research
USA

ABSTRACT

We performed a sequence of tests on a partially water-saturated sand sample contained in an x-ray-transparent aluminum pressure vessel that is conducive to x-ray computed tomography (CT) observation. These tests were performed to gather data for estimation of thermal properties of the sand/water/gas system and the sand/hydrate/water/gas systems, as well as data to evaluate the kinetic nature of hydrate dissociation. The tests included mild thermal perturbations for the estimation of the thermal properties of the sand/water/gas system, hydrate formation, thermal perturbations with hydrate in the stability zone, hydrate dissociation through thermal stimulation, additional hydrate formation, and hydrate dissociation through depressurization with thermal stimulation. Density changes throughout the sample were observed as a result of hydrate formation and dissociation, and these processes induced capillary pressure changes that altered local water saturation.

Keywords: hydrate formation, dissociation, porous medium, thermal stimulation, depressurization, x-ray computed tomography, capillary pressure

INTRODUCTION

To efficiently produce natural gas from hydrate reservoirs, an understanding of how hydrate and porous media behave upon dissociation is needed. This understanding must be gained using field, laboratory, and numerical modeling studies. Laboratory studies using pure hydrate and hydrate in porous media are needed, and detailed data on when and the location these processes occur within a sample is paramount to understanding measured phenomena. We used core-scale laboratory porous medium samples containing hydrate, and performed temperature and pressure measurements along with x-ray computed tomography (CT) imaging to quantify and visualize physical changes. Heat transfer (as defined by thermal properties), dissociation kinetics, and mass transfer (as effected by intrinsic and relative permeability) will all affect natural gas production from hydrates[1-6]. Our goals here were to increase our understanding of heat transfer and kinetics.

HYDRATE EXPERIMENTS

We formed and dissociated methane hydrate in partially water-saturated sand contained in an x-ray-transparent vessel. Temperature measurements were collected at four locations in the sample, and total system pressure was measured. All tests were performed at temperatures above 0^{o}C, and thus no water freezing occurred. The tests we performed included thermal perturbations of the partially saturated sand/water/gas (s/w/g) system, hydrate formation, three thermal perturbations (one within

* Corresponding author: Phone: (510) 486-4414, Fax: (510) 486-5686, E-mail: TJKneafsey@lbl.gov

the hydrate stability zone and two resulting in dissociation), a second hydrate formation, and final dissociation by depressurization and thermal stimulation.

Method

An x-ray transparent aluminum pressure vessel with an inside diameter of 7.62 cm and sample length of 25.4 cm was packed with moistened F110 Silica Sand (U.S. Silica, Berkeley Springs, West Virginia) (Figure 1). The sand, consisting of rounded to subangular quartz grains primarily in the 100–200 micron size range, was moistened with distilled deionized water and packed in the vessel, resulting in a porosity of 36% and a water saturation of 58%. The vessel contained four type-T thermocouples inserted through one of the end caps. Packing was performed from the opposite end, using metal tubing to maintain the thermocouple position during packing. The pressure vessel was enclosed in a heat exchanger composed of a PVC jacket through which a temperature-controlled water/propylene glycol solution was flowed. CT measurements were made at specified intervals using a modified Siemens Somatom HiQ CT scanner.

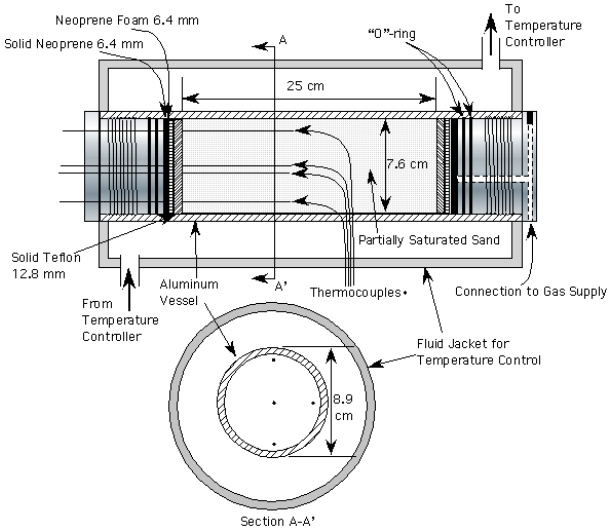

Figure 1. Vessel schematic.

We performed a sequence of tests on the sample (Figure 2) including thermal perturbations of the s/w/g system, hydrate formation (denoted by "1" in Figure 2), thermal perturbations of the sand/hydrate/water/gas (s/h/w/g) system including thermal stimulation (denoted by "3, 4, and 5" in Figure 2), a second hydrate formation (denoted by "6" in Figure 2), and dissociation from depressurization and thermal stimulation (denoted by "8" in Figure 2). Each test is described below.

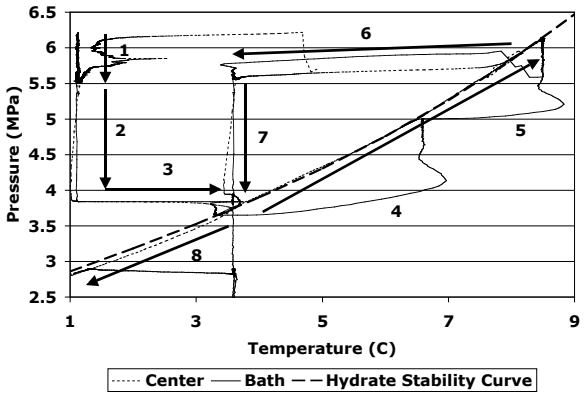

Figure 2. Experiment path: (1) hydrate formation, (2) stable depressurization, (3) stable temperature perturbation, (4) and (5) thermal-stimulation-induced dissociation, (6) second hydrate formation, (7) depressurization prior to dissociation, and (8) dissociation by depressurization/thermal stimulation. Hydrate is stable above the hydrate stability curve.

Thermal Tests

Heat transfer through the s/w/g system was investigated by abruptly changing the temperature of the bath fluid flowing through the heat exchanger. Temperature was both increased and decreased. Inverse modeling of these measurements is discussed in a companion paper [7].

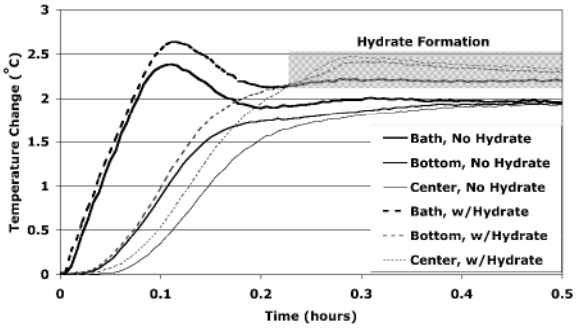

Figure 3. Comparison of the thermal response of the s/w/g system (no hydrate, solid curves) to the s/h/w/g system (with hydrate, dashed curves). "Bath" temperature is the temperature of the temperature-controlled fluid, "bottom" temperature is a mid-radius temperature, and "center" is the temperature in the center of the sample.

Figure 3 shows the temperature response for the s/w/g system (solid curves) as well as the temperature response for the s/h/w/g system (dashed curves). Observations from this figure are presented below.

Hydrate Formation

Methane hydrate was formed by increasing methane pressure in the vessel to 6.2 MPa while maintaining the temperature at 1.1°C (within the hydrate stability region). This method is similar to that used by Handa [8], and has been thought to produce hydrate that surrounds and cements mineral grains [9]. Upon pressurization, the temperature immediately rose as much as 3.5°C due to gas compression and hydrate formation. The initial formation subsided, and later was followed by rapid and then slow continued formation, with intermittent minor formation spikes. Hydrate was allowed to form over 28 hours, and was still slowly forming when the next test began. Based on pressure and temperature measurements, approximately 63% of the water in the sample was converted to hydrate (assuming 100% cage occupancy).

Thermal Tests with Hydrate

Prior to the thermal tests with hydrate present, the pressure in the system was reduced ("2" in Figure 2). Three abrupt temperature increases were then sequentially applied to the sample. The first was applied entirely within the hydrate stability region to examine the system response in the presence of hydrate ("3" in Figure 2). The second and third ("4" and "5" in Figure 2) were applied to induce dissociation. In these tests, the system was vented to a small vessel. When dissociation occurred, the pressure in the system increased, and the change in pressure was used to quantify the amount of dissociation.

The first thermal perturbation with hydrate present is shown as "3" in Figure 2, and dashed curves in Figure 3. Figure 3 shows that the temperatures in the sample increased faster with the hydrate present than without, indicating higher thermal conductivity. This indicates that the hydrate/water system provides a more thermally conducting bridge between sand grains. The first temperature increase (within the stability region) was unusual in that the sample temperature increased above the bath temperature (Figure 3) with concomitant pressure decline, indicating additional hydrate formation. The rate of hydrate formation increased as the conditions went from strongly stable towards the stability curve. This hydrate formation brought the system very close to the stability curve for the second temperature increase.

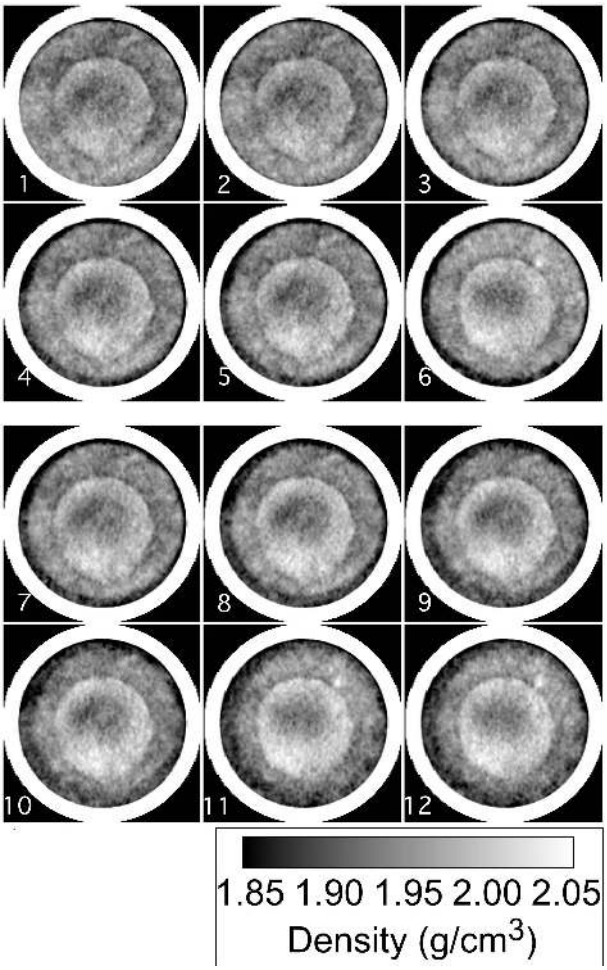

Figure 4. Calibrated CT scans from a single central location at twelve times over the thermal stimulation steps. 1 through 6 were collected during the second thermal increase, and 7 through 12 were collected during the third thermal increase.

The second and third temperature increases were similar to each other. Figure 4 shows the CT scans at a single central location over time calibrated to density and indicate the locations where changes occur. Initially, hydrate near the vessel wall began to dissociate (indicated by areas getting darker in color in Figure 4), and the dissociation front moved inwards towards the center with time. As dissociation continued, the system pressure increased. Because of the large thermal inertia of

the porous medium (i.e. low thermal conductivity and large specific heat), there is a delay in the system thermal response at the center of the sample following the change in the boundary temperature. The lower temperature near the sample center, coupled with the increase in pressure (resulting from hydrate dissociation at the sample periphery) and the relatively high permeability of the medium, lead to the increased stability of the hydrate near the sample center. This is indicated in Figure 2 by the location of the "center" curve above the "stability" curve, and in Figure 4 as a slight increase in density in the middle region.

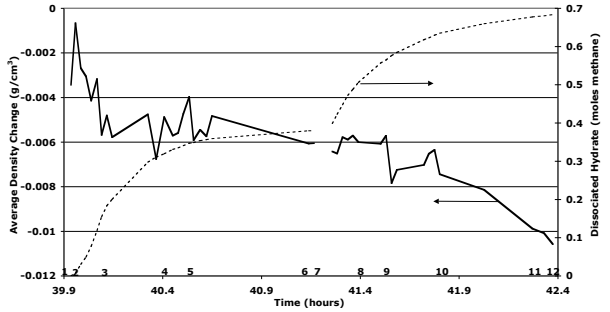

Figure 5. Changes in average density (heavy line), moles of methane produced from hydrate (dotted line). Numbers correspond to images in Figure 4.

Figure 5 shows the average change in density indicated by CT, in addition to the amount of hydrate dissociated during the two thermal stimulation steps ("4" and "5" in Figure 2). In "4," 25% of the hydrate present dissociated; in "5," an additional 22% of the original hydrate dissociated. As expected, the average density change and the dissociated hydrate curves tend to mirror each other. The mirror image is not perfect, however, because as the pressure increased later in the test, more methane was present in the gas phase, which affected x-ray attenuation.

Second Hydrate Formation

Following the temperature increases, hydrate was reformed by connecting the vessel to a pressurized methane reservoir and lowering the temperature to well within the stable zone ("6" in Figure 2). Figure 6 shows the density changes at a single central location over time during the hydrate formation, and Figure 7 shows the average density change from CT, as well as the amount of hydrate formed in the sample. The memory effect causes the reaction to occur very rapidly (on the order of one hour as opposed to many hours in the initial formation)[10-12]. The density increased greatly in the mid-radius zone (a ring away from the center and away from the vessel wall), and decreased in the remainder of the sample. We believe this is the result of hydrate formation changing capillary pressure and inducing water redistribution.

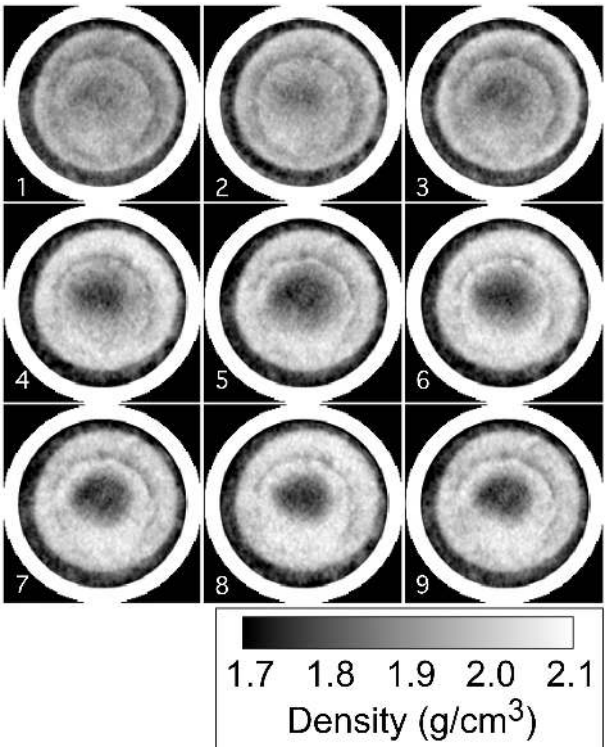

Figure 6. Calibrated CT scans from a single slice at nine times over the second hydrate formation. The increases in density are due to hydrate formation and water saturation changes.

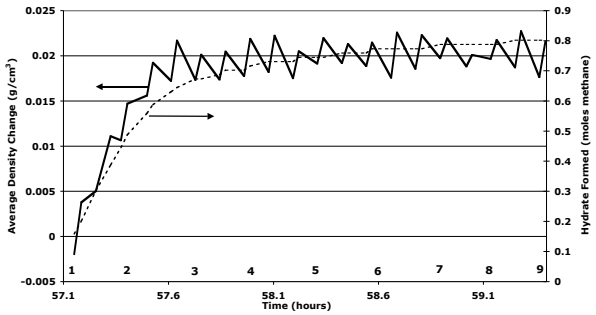

Figure 7. Average change in density (heavy line) and moles of methane converted to hydrate (dashed line) during the second hydrate formation. Numbers correspond to images in Figure 6.

Dissociation by Depressurization and Thermal Stimulation

After the second hydrate formation, the system pressure was lowered to just above the stability point and the system was allowed to equilibrate. Like the stable thermal test with hydrate present, as the system approached the stability point hydrate formed as indicated by a decrease in pressure and an increase in temperature that exceeded the bath temperature. Prior to the depressurization test, the system conditions were very close to equilibrium (3.75 MPa and 3.7°C). The system was then depressurized through a back-pressure regulator set to about 2.85 MPa (equilibrium temperature 0.95°C) to a Marriotte bottle, where the gas was collected and quantified. Upon depressurization, the sample temperature dropped below 1°C, despite the bath temperature being maintained at 3.6°C. Temperatures at the outer thermocouples increased slowly and monotonically towards the bath temperature. However, the temperature in the sample center remained near 1.3°C for about an hour and a half before rapidly climbing monotonically to the bath temperature.

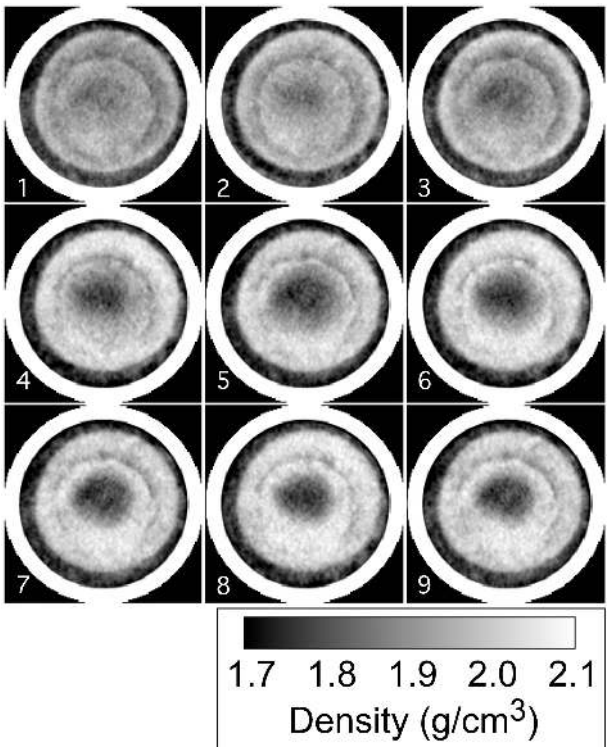

Figure 8. Calibrated CT scans from a single central location at nine times over the depressurization/thermal stimulation. The changes in density are the result of hydrate dissociation and water saturation changes.

Upon depressurization, dissociation occurred throughout the sample, resulting in the near-equilibrium temperature being established throughout. Because the temperature of the entire sample had dropped and the bath temperature remained steady, the subsequent dissociation was thermally induced, occurring as heat was transferred into the sample. Figure 8 shows the changes in density at a single central location over the course of the dissociation. The density changes between the first and second image are evident across the bright circle in the mid-radius region. From then on, the dissociation front moved radially inwards from the vessel wall.

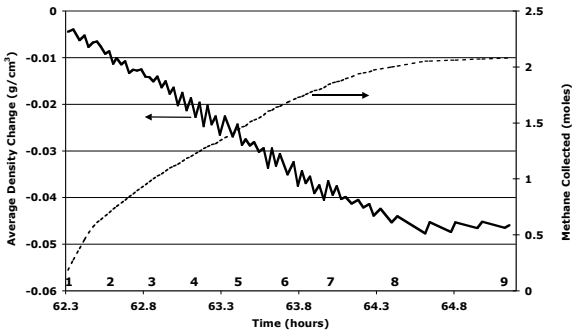

Figure 9. Average change in density (heavy line) and moles of methane hydrate dissociated (dashed line) during the depressurization/thermal stimulation. Numbers correspond to images in Figure 8.

Figure 9 shows the average density change over the dissociation process and the number of moles of methane collected. As with Figure 5, the two curves mirror each other. Because the pressure remains constant over this test, methane pressure does not affect the mirroring of the curves.

DISCUSSION

CT Scanning

The use of CT has provided a better understanding of how hydrate behaves in our experimental systems [13, 14] and also in natural samples [15, 16]. In these systems, CT enables us to determine the locations where processes occur, allowing better interpretation of measurements made on the bulk samples.

Prior to our using CT to investigate hydrate and porous medium behavior on formation and

dissociation of hydrate, our conceptual model consisted of water uniformly distributed throughout the sample in pendular structures between grains. This model did not consider the impact of hydrate on the capillary pressure-(water) saturation function of the combined sand/hydrate medium. This function is further complicated upon either hydrate formation or dissociation by the changing hydrate saturation, and is expected to be different for pore filling or cementing hydrate configurations.

Figures 5, 7, and 9 show the relative accuracy with which the averaged CT data can be used to indicate density changes, and these changes are directly related to the amount of methane consumed or produced by the processes occurring. This provides confidence in using the data to investigate bulk system behavior. Figures 4, 6, and 8 show us the locations where processes are occurring, allowing us to properly attribute the measurements to local changes, rather than to the bulk of the sample

Capillary Pressure and Saturation

In our CT imaging, we noticed density changes greater than those that could occur from hydrate formation or dissociation alone. Other processes that affect local density include saturation changes, mechanical deformation, and gas pressure. Of these, saturation has the greatest effect. In our tests, we believe these density changes are due to hydrate formation changing capillary pressure and causing water to flow.

The direction of the thermally induced dissociation ("4" and "5" in Figure 2) was from the outside towards the sample center. As it occurred and water was freed, the water moved towards the lower capillary pressure region in the center (where hydrate was present). This left the outer zone drier. On the second hydrate formation ("6" in Figure 2), little hydrate formation occurred in the outer zone. Most hydrate formation occurred in the more central zone, and less in the sample center. We think this occurred because the hydrate near the vessel wall formed rapidly, and because little water was present there, the capillary pressure at this location was not strongly changed. When the formation front reached the more saturated mid-radius zone, the hydrate formation changed the capillary pressure and caused water to flow from the sample center. Hydrate formation then proceeded towards the center, where water saturation was lower. Following the final dissociation by depressurization and thermal stimulation ("8" in Figure 2), water was again redistributed very similarly to the initial condition.

Thermal Data

Our measurements have allowed us to observe more rapid heat transfer in our sample with hydrate present than with only water. Because the thermal conductivities of water and hydrate are similar (hydrate 0.5 $Wm^{-1}K^{-1}$ [17], water 0.58 $Wm^{-1}K^{-1}$ [18]), and because for a constant water volume, hydrate has a greater volume, we expected heat transfer to be approximately the same for the s/w/g and s/h/w/g cases. It is apparent from Figure 3 that the thermal conductivity of the system with hydrate is higher than that without the hydrate. This may indicate a cementing type of hydrate configuration, however these data alone are insufficient to conclude this.

Modeling

The set of experiments described here provide a wealth of data for numerical modeling. Because of the complexity of the system and system changes that occur throughout the series, history matching or inverse modeling approaches will be needed. Modeling of one of the tests described is presented in a companion paper[7].

Kinetics

In the depressurization/thermal dissociation step ("8" in Figure 2), the temperature in the sample center (1.3°C) was clearly not the equilibrium temperature for the dissociation pressure (0.95°C). The actual pressures at which the hydrate dissociated in this test are not precisely known, however, and would have been higher than the measured system pressure because of the pressure needed to drive the generated methane through the connected pore space. We did not measure either the absolute or relative permeability of the system under test conditions. These parameters can be estimated, but additional measurements would be needed to allow us to determine the impact of dissociation kinetics on gas production.

CONCLUSIONS

We have collected an important data set that will provide insights into heat transfer in porous medium-hydrate systems, and hydrate dissociation kinetics. Using CT, we observed the locations where changes were occurring, enabling us to attribute bulk measurements to these locations instead of to the entire sample. The CT observations also enabled us to observe the effects of changes in saturation due to capillary pressure differences caused by hydrate formation and dissociation. These changes may strongly affect relative permeability, and need to be considered in experiment design.

ACKNOWLEDGEMENT

The authors wish to acknowledge Mike Kowalsky and Dan Hawkes for their helpful comments on reviewing this manuscript. This work was supported by the Assistant Secretary for Fossil Energy, Office of Natural Gas and Petroleum Technology, through the National Energy Technology Laboratory, under the U.S. DOE, Contract No. DE-AC03-76SF00098.

REFERENCES

[1] Kim, H.C., et al., Kinetics of Methane Hydrate Decomposition. *Chem. Eng. Sci.*, 1987. **42, No. 7**: p. 1645-1653.

[2] Clarke, M. and P.R. Bishnoi, Determination of the activation energy and intrinsic rate constant of methane hydrate decomposition. *Canadian Journal of Chemical Engineering*, 2001. **79**(1): p. 143-147.

[3] Moridis, G.J., Numerical Studies of Gas Production From Methane Hydrates. *SPE Journal*, 2003. **32**(8): p. 359-370.

[4] Moridis, G.J. and T. Collett, Gas Production from Class 1 Hydrate Accumulations, in *Recent Advances in the Study of Gas Hydrates*, C. Taylor and J. Qwan, Editors. 2004, Kluwer Academic/Plenum Publishers. p. 75-88.

[5] Moridis, G.J., et al., Numerical Studies Of Gas Production From Several Methane Hydrate Zones At The Mallik Site, Mackenzie Delta, Canada. *Journal of Petroleum Science and Engineering*, 2004. **43**: p. 219-239.

[6] Moridis, G.J., et al., Numerical studies of gas production from several CH4 hydrate zones at the Mallik site, Mackenzie Delta, Canada. *Journal of Petroleum Science and Engineering*, 2004. **43**: p. 219-238.

[7] Moridis, G.J., Y. Seol, and T. Kneafsey. Studies of reaction kinetics of the methane hydration reaction in porous media. in *Fifth International Conference on Gas Hydrates*. 2005. Trondheim, Norway.

[8] Handa, Y.P. and D. Stupin, Thermodynamic Properties and Dissociation Characteristics of Methane and Propane Hydrates in 70A Radius Silica Gel Pores. *J. Physical Chemistry*, 1992. **96**: p. 8599.

[9] Waite, W.F., W.J. Winters, and D.H. Mason, Methane hydrate formation in partially water-saturated Ottawa sand. *American Mineralogist*, 2004. **89**: p. 1202–1207.

[10] Sloan, E.D., et al., Quantifying hydrate formation and kinetic inhibition. *Industrial and Engineering Chemistry Research*, 1998. **37**: p. 3124.

[11] Schroeter, J.P., R. Kobayashi, and M.A. Hildebrand, Hydrate Decomposition Conditions in the System H2S-Methane-Propane. *Ind. Eng. Chem. Fundam.*, 1983. **22**: p. 361-364.

[12] Uchida, T., T. Ebinuma, and H. Narita, Observations of CO2-hydrate decomposition and reformation processes. *Journal of Crystal Growth*, 2000. **217**(1/2): p. 189-200.

[13] Tomutsa, L., et al. X-ray Computed Tomography Observation of Methane Hydrate Dissociation. in *SPE Gas Technology Symposium*. 2002. Calgary, Alberta, Canada.

[14] Freifeld, B.M., et al., Use of Computed X-Ray Tomographic Data for Analyzing the Thermodynamics of Dissociating Porous Sand/Hydrate Mixture. *Proc. 4th International Conference on Gas Hydrates, Yokohama May 19-23, 2002*, 2002: p. 750-755.

[15] Uchida, T., S. Dallimore, and J. Mikami, Occurrences of natural gas hydrates beneath the permafrost zone in Mackenzie Delta visual and X-ray CT imagery. *Annals of the New York Academy of*

Sciences, 2000. **912**(Gas Hydrates): p. 1021-1033.
[16] Mikami, J., et al., Dissociation of natural gas hydrates observed by X-ray CT scanner. *Gas hydrates, challenges for the future*, 2000. **NYAS 912**: p. 1011.
[17] Cook, J.G. and D.G. Leaist, An Exploratory Study of the Thermal Conductivity of Methane Hydrates. *Geophysical Research Letters*, 1983. **10(5)**: p. 397-399.
[18] Incropera, F.P. and D.P. DeWitt, Fundamentals of Heat Transfer. 1981, New York: John Wiley and Sons. 819.